Numerical investigation of the stability criteria for the breathing mode in Hall Effect Thrusters

IEPC-2017-265

Presented at the 35th International Electric Propulsion Conference
Georgia Institute of Technology – Atlanta, Georgia – USA
October 8–12, 2017

Ethan T. Dale* and Benjamin Jorns†
University of Michigan, Ann Arbor, MI, 48105, USA

Kentaro Hara‡
Texas A&M University, College Station, Texas, 77843, USA

Several zero-dimensional models of the Hall thruster breathing mode were investigated analytically and numerically to determine the criteria for the onset of the instability. The breathing mode is a common instability observed in Hall thrusters that is often reproduced with multi-dimensional simulations but has not been accurately captured with a 0D model of the device. To date there is little physical insight into the energy source for this instability, and there are no analytical criteria for its growth. A 0D model adapted from the work of Hara et al.[1] is examined with numerical simulations and linear perturbation analysis for the systematic addition of electron temperature, electric field, and ionization region length perturbations. It is found through numerical experiments that temperature dependence alone leads to a stable system. Adding E perturbations similarly does not allow for any unstable behavior. By removing temperature dependence and adding perturbations in L_{iz}, the system is found to be unconditionally unstable, indicating that a 0D model may successfully recover breathing mode oscillations. An approximation for the growth rate for this system is derived and the physical implications discussed.

*Ph.D. Candidate, Department of Aerospace Engineering, etdale@umich.edu.
†Assistant Professor, Department of Aerospace Engineering, Co-Director of Plasmadynamics and Electric Propulsion Laboratory, bjorns@umich.edu.
‡Assistant Professor, Department of Aerospace Engineering, khara@tamu.edu.

Nomenclature

α = anomalous collision scaling factor
γ = angular growth rate
ϵ_{iz} = ionization energy
ϵ_w = electron energy lost to the wall
ζ = damping ratio
η = resistivity
κ = ionization coefficient power factor
Λ = electron relaxation length
ν = total electron collision frequency
ν_w = electron-wall collision frequency
ξ_{iz} = ionization rate coefficient
σ = secondary electron yield
τ = exponential decay time
ϕ_w = wall sheath potential
χ = ionization cost
ω = observed angular frequency
ω_n = natural angular frequency
Ω = Hall parameter
a = neutral density ratio
b = neutral length ratio
B_r = peak radial magnetic field strength
e = electron charge
E = axial electric field
j = current density
ℓ = neutral length
L_{ch} = channel length
L_{iz} = ionization region length
n = plasma density
n_{int} = injected neutral density
n_n = neutral density
T_e = electron temperature
u_B = Bohm speed
u_{bm} = ion beam velocity
u_e = electron velocity
u_f = ionization front velocity
u_i = ion velocity
u_n = neutral velocity
x = axial position

I. Introduction

Hall effect thrusters are increasingly becoming an attractive option for in-space propulsion, both in Earth orbit and for deep space missions.[2] However, as these thrusters are scaled to higher power to enable a greater variety of missions, ground testing becomes more difficult and the ability of laboratory performance to predict performance on orbit becomes more suspect. Background pressure effects[3] and electrical facility interactions[4] have already been identified as influencing Hall thruster operation in laboratory tests. Naturally, the role of simulation must increase in the design of these devices to accommodate for this shortcoming until experimental techniques improve. However, the use of simulations is currently limited as several aspects of the physics governing the operation of Hall thrusters are still unclear. For example, electron mobility is anomalously high in certain regions of the discharge, and although expensive full particle-in-cell (PIC) simulations appear to capture this transport as a result of azimuthal turbulence,[5] simulations with fluid electrons must be artificially "tuned" to match experimental performance.[6] Similarly, another area where the modern understanding of Hall thrusters falls short concerns the stability of these devices, particularly with regard to the ubiquitous so-called "breathing mode". This instability is characterized by large-scale ($\sim$100%) oscillations in discharge current, which poses the concern that such strong global changes in the thruster plasma may correspond to fundamental changes in the operation of the device throughout a breathing cycle. While many simulations[7–12] can reproduce the phenomenon, these codes are neither self-consistent nor predictive. To date, only empirical scaling laws are available for determining the onset of the breathing mode. To allow Hall thruster technology to mature, it is important that these unclear phenomena be studied to improve the fidelity of thruster codes and to determine whether any simple scaling laws for the breathing mode exist.

Toward that end, there has been progress made with Hall thruster simulations and theoretical analysis. With the former, the breathing mode has been reproduced and its dependence on different operating parameters has been examined.[8,9] This has yielded a rough physical explanation of the process, but it has not provided insight into the precise physics controlling it, nor the criteria for its growth. Analytical approaches have leveraged this physical understanding to estimate properties of the breathing mode like its frequency, but again no coherent description of its growth rate has been formulated.[13] These simple models have ranged in complexity, some only including neutral and ion continuity equations,[7] while others include electron energy conservation and thus depend on electron temperature.[1] However, no simple onset criteria have been yielded by any 0D model to date.

The goals of the work described in this paper were to develop analytical criteria for growth of the breathing mode instability, and to leverage those criteria to gain an understanding of the mechanisms controlling it. To accomplish this, this paper is organized in the following way. First we define a simple 0D model based on previous studies by Hara et al.[1] We then gradually introduce time-dependent forms for electron temperature, electric field strength, and ionization region length, which is equivalent to adding new energy sources that may drive instability. For each new perturbed quantity, the system is evaluated with a preliminary sample of numerical simulations, followed by a more extensive map of numerical cases, and concluded with a linear perturbation analysis.

II. Background

In this section, previous numerical, experimental, and analytical investigations of the breathing mode are discussed. This review is by no means exhaustive, as many codes are reported recovering the breathing mode without special attention, and many thrusters operate in oscillatory modes that are considered nominal.

Early hybrid-PIC simulations by Fife et al. reproduced breathing-like oscillations at frequencies comparable to those observed experimentally.[7] These 2D simulations described the breathing process as a cyclical depletion and replenishment of neutrals in the discharge channel. A 1D hybrid-kinetic code created by Boeuf and Garrigues similarly demonstrated breathing as being a cycle involving neutrals getting depleted upstream as ionization shifts in that direction, and then the channel refilling with neutrals once the enhanced ionization region collapses.[8] This study also showed that discharge current oscillation amplitude increased with voltage, with the discharge quiescent at low voltages. Similar 2D hybrid-PIC codes also showed increasing oscillation strength with increasing magnetic field strength.[9] The general breathing mode process described here has also been demonstrated with 1D fluid codes,[10] full PIC codes,[11] and 2D hybrid-kinetic models.[12]

There exists considerable literature describing the breathing mode experimentally across a wide variety of thrusters. Even though the trends that can be gleaned from these accounts are not always consistent, some trends do seem to hold true for many modern thrusters. For example, it has been observed with the H6, H6MS, and NASA-300MS-2 that decreasing magnetic field strength increases oscillation amplitude.[14] Background pressure studies have shown that discharge current oscillation amplitude increases with pressure, and that breathing frequency varies non-monotonically with pressure but increases with voltage.[3] Mapping of oscillation strength over discharge current, discharge voltage, and magnetic field strength for the 12.5-kW HERMeS thruster showed the discharge current oscillation amplitude increased with discharge voltage, increased with flow rate (discharge current), and decreases with background pressure,[?] which is echoed in studies of the H6.[15] Of particular interest are the results of time-resolved laser-induced fluorescence studies, which show periodic changes in the peak ion velocity, suggesting that the electric field profile is distorting as an "ionization front" travels throughout the channel.[16]

The breathing mode is often referred to as "loop" or "circuit" oscillations in older Russian literature due to its perceived dependence on the thruster electronics.[13] However, one of the first attempts at describing it analytically to complement hybrid-PIC simulations, performed by Fife et al.,[7] disregarded electrical effects and used a 0D Lotka-Voltera (predator-prey) model with neutral and ion continuity equations. With this formulation, they estimated the frequency of the oscillations as,

$$\omega = \frac{\sqrt{u_i u_n}}{L_{iz}} \,. \tag{1}$$

However, this model neither predicts growth nor does it capture outflow of neutrals from the discharge channel. Additionally, it relies on an ill-defined "ionization length" that cannot be modeled without one-dimensional considerations. Barral and Ahedo used a fluid model to describe the breathing mode as the combination of a standing wave and a traveling wave, with the predicted frequency closely matching that of Fife.[17] Hara et al. added a dependence on electron temperature to the predator-prey model and observed the possibility of growth in numerical experiments.[1]

In summary, the breathing mode is captured by many different codes, although studies of trends in oscillation amplitude with operating parameters is limited. Experimental evidence suggests that breathing mode is sensitive to a wide range of operating parameters, including discharge voltage, magnetic field strength, and background pressure. Analytical models are either too limited or rely on numerical results, preventing them from giving insight into the onset criteria of the instability.

III. 0D Model

In this section, the 0D model with which we investigated the breathing mode is outlined. First, the complete set of governing equations are presented. Next, the general approach with which different subsets of these equations are explored is described. Finally, the specific numerical setup used in the simulation of different subsets of equations is detailed.

A. Governing Equations

In this work, we consider a 0D Hall thruster discharge channel, encompassing the ionization and acceleration regions. This is illustrated in Fig. 1, where particle fluxes are shown at the boundary of the 0D system. The fundamental equations are neutral continuity, ion continuity, ion momentum conservation, and electron energy conservation, shown as Eqs. (2)-(5).

$$\frac{dn}{dt} = \xi_{iz} n n_n - \frac{u_i n}{L_{ch}} - \frac{2 u_w n}{R} \tag{2}$$

$$\frac{dn_n}{dt} = -\xi_{iz} n n_n - \frac{u_n n_n}{L_{ch}} + \frac{u_n n_{int}}{L_{ch}} \tag{3}$$

$$\frac{dn u_i}{dt} = \frac{e}{m_i} n E - \frac{{u_i}^2 n}{L_{iz}} \tag{4}$$

$$\frac{d}{dt}\left(\frac{3}{2} n T_e\right) = -\frac{5}{2}\frac{n T_e u_e}{L_{iz}} - n u_e E - n \epsilon_w \nu_w - n n_n \xi_{iz} \epsilon_{iz} \chi \tag{5}$$

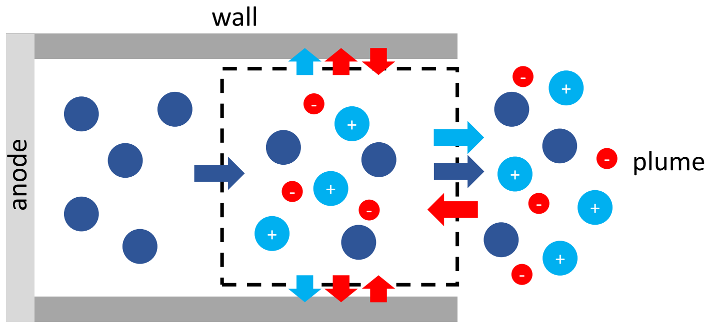

Figure 1. A physical picture of the temperature-dependent model, where the 0D system is contained within the dashed box. Neutral (dark blue), ion (light blue), and electron (red) fluxes are shown at the borders of the 0D box.

The ion continuity equation accounts for convection out of the thruster, radial losses to the walls, and ionization. The neutral continuity equation includes inflow from the anode, convection out of the thruster, and ionization. The ion momentum equation considers acceleration by a constant electric field, E, and convection out of the thruster. In the steady state, this equation dictates that the ion velocity is equal to the beam velocity (the ion velocity after acceleration through the entire discharge volage). The electron energy equation includes convection of electrons into the thruster, Joule heating, wall collision losses, and inelastic collision losses. The final term considers ionization collisions but is scaled by a cost factor χ to account for excitation. The wall collision frequency ν_w, the electron energy lost to the wall per collision ϵ_w, and the wall sheath potential ϕ_w follow forms used by Barral and Ahedo[18] and are given by Eqs. (6)-(8). Additionally, an effective ionization length is defined by comparing Eq. (3) to the predator-prey form neglecting wall losses, and this definition is shown in Eq. (9). As a result, L_{iz} has a dependence on T_e and u_i, which in the steady state are themselves dependent on other operating parameters.

$$\nu_w = \frac{u_w}{R}\frac{1}{1-\sigma} \tag{6}$$

$$\epsilon_w = 2T_e + (1-\sigma)\phi_w \tag{7}$$

$$\phi_w = -T_e \log\left(\frac{1-\sigma}{\sqrt{\frac{2\pi m_e}{m_i}}}\right) \tag{8}$$

$$L_{iz} = L_{ch}\left(1 + 2\frac{u_B}{u_i}\frac{L_{ch}}{R}\right)^{-1} \tag{9}$$

To capture fluctuations in E, a simple Ohm's law ignoring pressure terms can be included in the model:

$$E = \eta\Omega^2 j = \frac{-eu_e B_r^2}{\nu m_e} \ . \tag{10}$$

The collision frequency is the sum of electron-neutral, Coulomb, and anomalous collisions, where the last contribution was Bohm-like and scaled with parameter α. In this way, α and either E or u_e become the independent variables for this model.

Finally, changes in ionization region length can be accounted for. To do this, first it is assumed that the breathing mode occurs in the ionization region, which oscillates over time in density and spatial extent. The width of the ionization region is strongly dictated by one-dimensional effects, but changes in size due to the breathing mode can be modeled separately. Allowing the ionization region to deform may also be used to capture spatial effects although in this implementation it does not depend on any steady-state plasma gradients except for that of neutral density.

To model changes in ionization length, one can imagine the ionization region being an isolated block of plasma, where the upstream edge ("ionization front") is a transition from pure neutral gas to a mixture of plasma and neutrals. This is depicted in Fig. 2, where there is a front that merges into a region of constant ion density that eventually accelerates out of the thruster. A 0D neutral continuity equation can be written in the frame of reference of this upstream ionization edge. However, the transformation to this new frame of reference must first be considered.

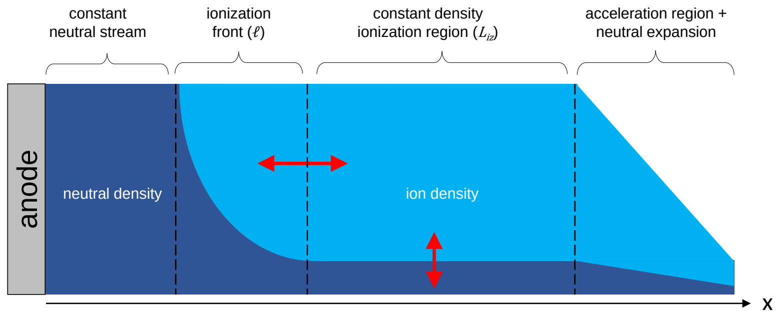

Figure 2. Growth rate as a function of the neutral density ratio a and neutral-ionization length ratio b.

The edge is expected to accelerate since it presumably oscillates back and forth, and thus this frame of reference is non-inertial. As a result, a Galilean transformation is not appropriate. The transformation required to describe the time rate of change of scalar quantity r in the ionization front frame of reference (denoted with subscript "f") can be shown as,

$$(dr)_f = dt\frac{\partial r}{\partial t} + dt\frac{dx}{dt}\frac{\partial r}{\partial x} \, , \tag{11}$$

$$\left(\frac{dr}{dt}\right)_f = \frac{\partial r}{\partial t} + u_f\frac{\partial r}{\partial x} \, . \tag{12}$$

Intuitively, this transformation indicates that the rate at which a quantity changes is a combination of the laboratory frame rate (the first term on the righthand side) and the change due to moving through the laboratory frame gradient (the second term on the righthand side).

In the frame of reference of the ionization front, the time rate of change of neutral density can be expressed as Eq. 13. Given that neutral continuity in the laboratory frame can be expressed as Eq. 14, Eq. 13 becomes Eq. 15, which represents neutral continuity in the ionization front frame. Since the front is imagined traveling along an undisturbed stream of neutrals, the first term is zero. If the drop in neutral density across the front is assumed to be exponential, a gradient length ℓ can be assigned, simplifying the second term. The front velocity can be solved for explicitly, yielding Eq. (16).

$$\left(\frac{dn_n}{dt}\right)_f = \frac{\partial n_n}{\partial t} + u_f\frac{\partial n_n}{\partial x} = 0 \tag{13}$$

$$\frac{\partial n_n}{\partial t} = -u_n\frac{\partial n_n}{\partial x} - nn_n\xi \tag{14}$$

$$\left(\frac{dn_n}{dt}\right)_f = -u_n\frac{\partial n_n}{\partial x} - nn_n\xi + u_f\frac{\partial n_n}{\partial x} = (u_f - u_n)\frac{\partial n_n}{\partial x} - nn_n\xi = 0 \tag{15}$$

$$u_f = u_n - n\xi n_n\left(\frac{\partial n_n}{\partial x}\right)^{-1} \approx u_n - n\xi\ell \tag{16}$$

This form for the front velocity has a simple physical interpretation. The speed at which the ionization region moves upstream is the difference between the speed at which "fuel" enters, u_n, and the speed at which it is consumed by ionization, $n\xi\ell$.

The ionization length L_{iz} can be described as in Eq. (17), where it is assumed that small perturbations in plasma density are sinusoidal in time such that $n = n_0 + n'$ where $n' = \tilde{n}\exp(-i\omega t)$ and $\tilde{n}$ is the small oscillation amplitude. In the steady state, $u_f = 0$ and $u_n - \ell n_0\xi = 0$. The perturbed form of the inverse of the ionization length, which is of more practical interest, can be expressed as Eq. (18).

$$L_{iz} = L_{iz,0} - \int u_f dt = L_{iz,0} + \int n'\xi\ell dt = L_{iz,0} + i\frac{\xi\ell}{2\omega}n' \tag{17}$$

$$\left(\frac{1}{L_{iz}}\right)' \approx -i\frac{\xi\ell}{{L_{iz,0}}^2\omega}n' \tag{18}$$

Physically, these equations imply that changes in the ionization region length lag behind changes in ion density by 90°. In a linear sense, perturbations in the inverse of L_{iz} lead changes in n by 90°. Qualitatively, this can be understood as the ionization region stretching or compressing in response to variations in bulk ion density, with a lag occurring because this stretching is a function of these variations.

B. General Approach

In this work, several subsets of the governing equations outlined in the previous section are examined in terms of stability. A common procedure is followed and is described in this section. First, numerical simulations of the system are conducted for a limited set of input parameters to qualitatively identify any trends in the response. This includes examining whether each time-dependent quantity damps and whether the damping behavior between them is different. Next, a map of damping behavior is produced from numerical simulations over a wide range of input parameters to evaluate the breadth of the conclusions on stability made from the preliminary simulations. Finally, a linear perturbation analysis is performed on the system as an even broader assessment of stability.

For the linear analysis, n_n, n, u_i, and T_e can be treated as perturbation quantities, and E and L_{iz} depend on perturbed quantities. The determinant of the linearized matrix of equations is a polynomial in ω, and its roots can be solved to find ω explicitly. A positive growth rate corresponds to $\mathrm{Im}(\omega) > 0$ and suggests that the instability will be able to grow and non-linearly saturate, and thus be observable in real thrusters. Although the roots for third and fourth order polynomials can be found exactly, the forms are often too complicated to be useful for the equations involved here. As a result, the stability of higher order systems can be judged using the Routh-Hurwitz theorem.[19] Specifically, for a polynomial in the complex plane, this theorem provides sufficient and necessary criteria for all roots to be in the left half-plane. For a linear perturbation analysis where a perturbation quantity q' has the form $\tilde{q}\exp(-i\omega t)$, all ω must be substituted with $-i\omega$ to apply this theorem for determining linear stability.

C. Numerical Setup

The numerical simulations we performed used input parameters for the SPT-100.[20] The channel length and width are 2.5 and 2 cm, respectively. A discharge current and voltage of 4.5 A and 300 V respectively were used, which corresponds to the nominal 1.35 kW operating condition. A current utilization efficiency between 50% and 100% is assumed to allow the estimation of u_e/u_i, following Hara et al.[1]

IV. Results

A. Case I

The simplest subset of the governing equations is the neutral and ion continuity equations alone. For simplicity, the radial ion losses are disregarded and L_{ch} is more appropriately treated as L_{iz}. Because the linearized matrix determinant is only second order, it is sufficient to judge stability from a linear perturbation analysis. It has been shown in the literature[1] that the growth rate is,

$$\gamma = -\frac{1}{2}\frac{n_{int}}{n_{int}-n_n}n\xi \ , \tag{19}$$

and thus all physical solution are damped.

B. Case II

Next, the ion momentum conservation equation Eq. (4) can be included to the model of Section IV A. Again, the system is simple enough that numerical simulations are unncessary and the Routh-Hurwitz method can be used to judge linear stability. The determinant of the linearized matrix of this system is a third-order polynomial in ω, shown in Eq. (21). The condition for stability is given by,

$$u_i < L_{iz}n_{int}\xi_{iz} \ , \tag{20}$$

which is guaranteed by the construction of the system. Thus, the system is always damped. This result suggests that the ion momentum equation either has little impact on the system or contributes damped poles to it. The former agrees with the observation that the breathing frequency scales closer to the neutral transit time than the ion transit time, which is generally expected to be an order of magnitude larger,[13] and thus ions respond almost instantly to changes in the plasma during breathing.

$$\frac{2u_i u_n(-u_i + L_{iz} n_{int}\xi_{iz})}{L_{iz}^2 L_{ch}} + \frac{u_n(-u_i + 2L_{iz} n_{int}\xi_{iz})}{L_{iz} L_{ch}}\omega + \left(\frac{u_i}{L_{iz}} + \frac{L_{iz} n_{int} u_n \xi_{iz}}{L_{ch} u_i}\right)\omega^2 + \omega^3 = 0 \tag{21}$$

C. Case III

By adding the electron energy conservation equation Eq. (5), the time-dependent parameters of the system now include n_n, n, u_i, and T_e. The determinant of the linearized matrix for this system is fourth order in ω, and thus is too complicated to examine by a linear perturbation analysis alone. As described previously, investigating the system's stability will begin with numerical simulations, which will then be compared to a a slightly broader numerical linear analysis.

1. Preliminary Numerical Simulations

The full nonlinear equations are evaluated for a few values of u_e/u_i between 0.5 to 5 and the results over 0.5 ms are shown in Fig. 3. The response is damped for all cases examined. In Fig. 4 the T_e plot is normalized by the steady state value so that the shape of the response can be compared for different inputs, and from this it is clear that T_e fluctuates very little compared to other quantities. This implies that the electron energy equation may be poorly coupled to the rest of the system since there are many conditions where T_e remains nearly steady or is only weakly perturbed. If the electron energy equation is playing such a limited role in the time response of the system, this model may be unconditionally stable since we proved in Section IV B that the continuity equations together with the ion momentum conservation equation are always damped.

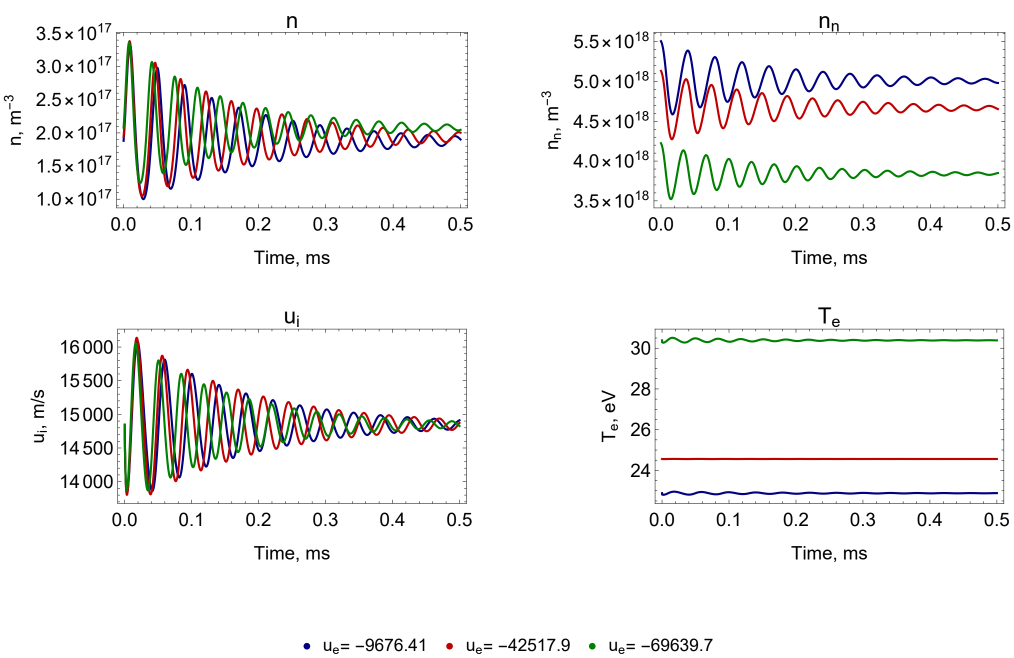

Figure 3. The time response of the neutral density, ion density, ion velocity, and electron temperature for various electron velocities.

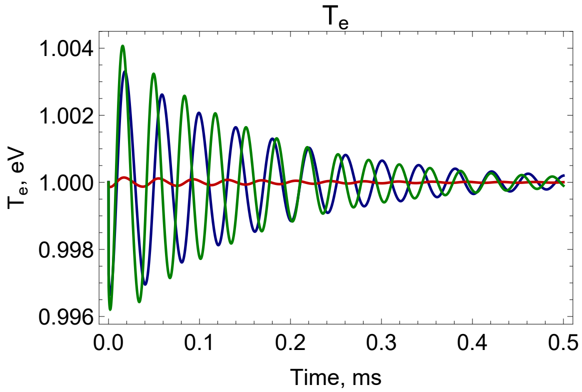

Figure 4. The normalized time response of the electron temperature for various electron velocities.

2. Extensive Numerical Map

To verify the trends observed previously, numerical simulations are performed for a wide range of input parameters and the stability is summarized with the damping ratio of the ion density time response. The damping ratio ζ, defined as

$$\zeta = (\tau\omega_n)^{-1} \approx (\tau\omega)^{-1} \ , \tag{22}$$

is calculated for a 10% initial perturbation of the neutral density, where the natural frequency of the system was approximated with the observed frequency for simplicity. A harmonic oscillator is critically damped for $\zeta = 1$, undamped for $\zeta = 0$, and growing for $\zeta < 0$. Fig. 5 shows these values and demonstrates that they are all positive, and thus the system is stable over a wide range of inputs. The limits in u_e/u_i are dictated by the stiffness of the system, which generally means that the steady-state parameters become unphysical (e.g. $T_e < 0eV$) or the simulation is numerically unstable outside the plotted domain. This domain therefore represents the range of input parameters of physical interest for the chosen operating condition.

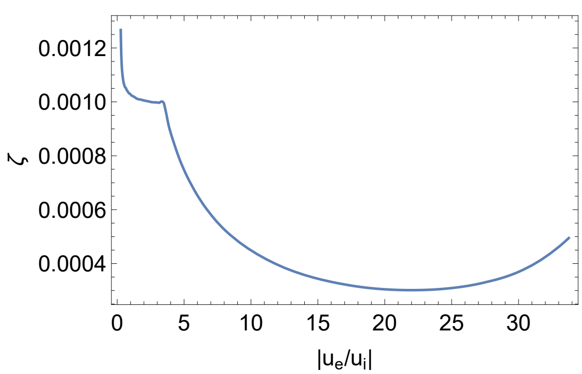

Figure 5. The damping ratio of the time response of the system for varying electron velocity.

3. Linear Analysis

A linear analysis can be performed using the perturbation forms of Hara et al.,[1] yielding the linearized matrix equation shown in Eq. (23), where κ is the power relating ξ_{iz} to linear perturbations in T_e, and Λ is defined in Eq. (24).

$$
\begin{bmatrix}
-i\omega & -n\xi_{iz} & \frac{n}{L_{ch}} & -n\frac{u_i}{L}\frac{\kappa}{T_e} \\
\frac{u_i}{L} & -i\omega + \frac{n_{int}}{n_{int}-n_n}n\xi_{iz} & 0 & n\frac{u_i}{L}\frac{\kappa}{T_e} \\
-i\omega u_i & 0 & n\left(-i\omega + \frac{2u_i}{L}\right) & 0 \\
-i\omega\frac{3}{2}T_e & n\xi_{iz}\chi\epsilon_{iz} & 0 & n\left(-i\frac{3}{2}\omega + \Lambda\right)
\end{bmatrix}
\begin{bmatrix} \tilde{n} \\ \tilde{n_n} \\ \tilde{u_i} \\ \tilde{T_e} \end{bmatrix} = \mathbf{0} \tag{23}
$$

$$
\Lambda \equiv \frac{3}{2}\frac{\epsilon_w}{T_e}\nu_w + \frac{u_i}{L}\frac{\kappa}{T_e}\chi\epsilon_{iz} + \frac{5}{2}\frac{u_e}{L} \ . \tag{24}
$$

The resulting polynomial given by the determinant of the linearized matrix is fourth order, which generally precludes any analytical judgment of stability. Alternatively, the growth rate and real frequency can be computed numerically for a given thruster and operating condition.

Fig. 6 shows representative numerical results for the SPT-100. All roots were damped, so only those with definite real and complex parts are shown. The only independent variable is the electron-ion velocity ratio, and it can clearly be seen that the growth rate is always negative and asymptotically approaching zero for stationary electrons. Previous work by Hara et al.[1] showed similar plots as a function of electron temperature, and although this may highlight that the model nearly predicts a region of positive growth, it is clear from Fig. 7 that the steady state T_e line never intersects the growing region. A linear perturbation analysis by definition is only valid around the steady state condition, thus this model does not predict linear growth for this case. However, because this system is intractable to evaluate analytically, it cannot be said that the system is stable for all conditions. It is also important to note that the range of u_e/u_i shown in the figure is far wider than that considered typical from the current utilization efficiencies expected for a SPT-100 or more modern Hall thrusters.

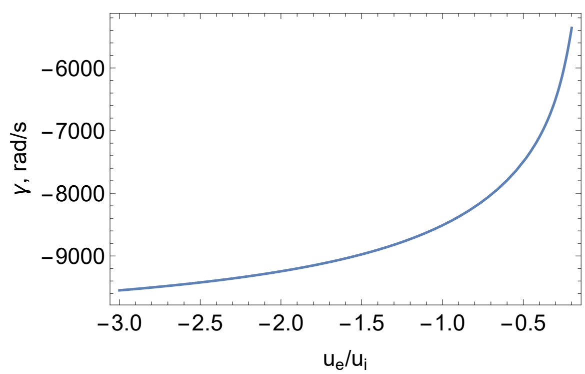

Figure 6. The growth rate as a function of the electron-ion velocity ratio..

D. Case IV

To improve the coupling of T_e to the rest of the system, Ohm's law can be added to the model. This allows the electric field to be expressed in terms of electron velocity and the total collision rate, which is a function of several time-independent parameters. In this way, E becomes a time-independent quantity, introducing another potential source of instability.

1. Preliminary Numerical Simulations

Fig. 8 shows the time response of the system as a function of u_e and α. The behavior is damped for these sample cases. Fig. 9 shows the T_e response normalized, as in Fig. 4. The curves show very small oscillation amplitudes, indicating that T_e coupling is not improved. This suggests that even including Ohm's law does not induce large perturbations in T_e, and including perturbations in E does not induce instability.

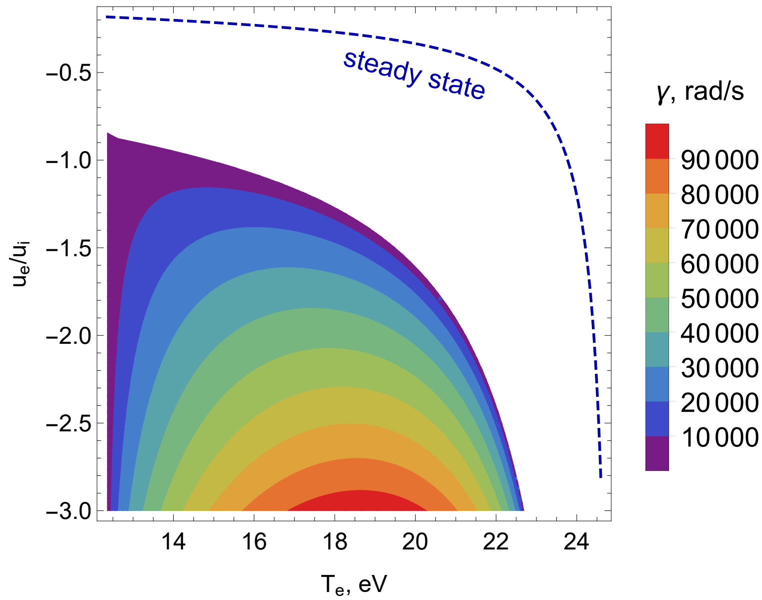

Figure 7. The growth rate as a function of the electron-ion velocity ratio (colored region), and the steady-state electron temperature (blue line). The white region corresponds to zero or negative growth rates.

2. Extensive Numerical Map

By defining a nominal discharge current, current continuity couples u_e to u_i and n such that α is a function of u_e. As a result, only one input parameter, u_e is required for this model with a given discharge current. Fig. 10 shows this relationship for a SPT-100. The limits of u_e in this plot are dictated by the stiffness of the system of equations. Fig. 10 shows the damping ratio for a range of u_e and α that are close to those for a nominal discharge current of 4.5 A. Everywhere the response is damped, and thus the system is everywhere stable. The discharge current curve is superimposed on the damping ratios in Fig. 10 for context. It should be noted that the damping ratios do not cover the full extent of the discharge current curve because the simulations became numerically unstable in certain extremes of this range. Even so, we conclude from Fig. 10 that even including Ohm's law into the temperature-dependent model does not induce instability for a nominal discharge current in this case.

3. Linear Analysis

The linear analysis for this system is similar to that of D, except the Ohm's law definition of E introduces perturbation terms to the linearized matrix. For ranges of u_e and α similar to the numerical simulation map in Fig. 10, the growth rate yielded by the linear analysis is nowhere positive. To demonstrate this, the growth rate of roots with finite positive real frequency is shown in Fig. 11. It is clear that the growth rate is always damped, supporting the findings of the numerical simulations.

E. Case V

A model incorporating time-dependent T_e and E terms was incapable of producing instability for a range of input parameters corresponding to a nominal discharge current. And based on the spatial dependence of many of the parameters for this model, any unstable marginal cases for the SPT-100 conditions considered here are not expected to be meaningful. The next step would naturally be to include ionization length perturbations in the the model of Section IV D. However, this would further complicate an already analytically intractable model, so the electron energy conservation equation (which contains E perturbations) and the damping ion momentum conservation equation are removed before including a L_{iz} perturbation form. The rationale for this approach is as follows: if perturbations in L_{iz} alone are shown to make the system unstable, any additional physical processes are not of primary importance for capturing the breathing mode

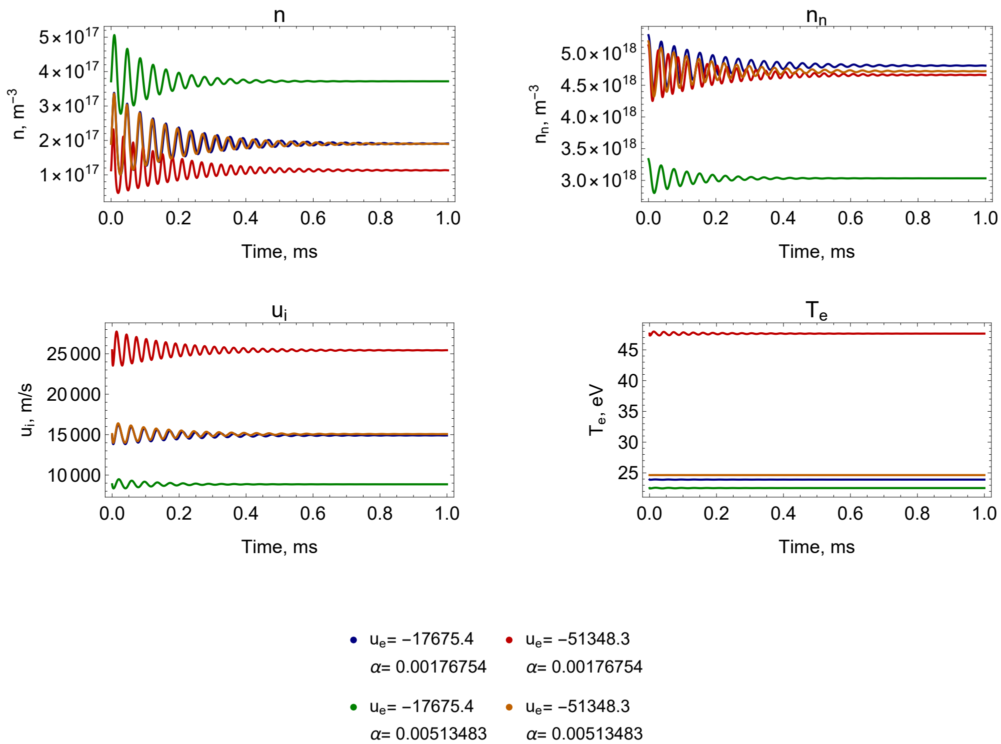

Figure 8. The time response of the system with Ohm's law included.

and only serve to add conditions to the instability; conversely if the system is stable, we do not expect L_{iz} perturbations to make a more complicated system unstable. These assumptions are unproven in this work but embraced for the sake of simplicity.

Instead of adding L_{iz} perturbations to the model of Section IV D, only the ion and neutral continuity equations are retained, as in Section IV A. This is done to make the system more tractable for linear perturbation analysis.

1. *Preliminary Numerical Simulations*

A sample numerical simulation of the full nonlinear equations is shown in Fig. 12. As can be observed, within 1 ms all quantities are oscillating and growing continuously, and the frequency is approximately 14 kHz at 1 ms. The nonlinear oscillations in ionization length and ion density are in phase, which is consistent with results from more sophisticated simulations.[8]

Since this system is observed to be unstable and is simple enough for analytical linear analysis, a more extensive set of numerical simulations is unnecessary.

2. *Linear Analysis*

The linearized matrix equation based on this system is shown in Eq. (25). For simplicity, . All quantities are steady-state. The roots of the determinant of the matrix must be found, and this determinant is given by Eq. (26). An exact analytical form for the roots of ω based on Eq. (26) exists but is much too complicated to be useful for judging the stability of the system.

$$\begin{bmatrix} \dfrac{au_n}{L_{iz}} - i\omega & \dfrac{u_i}{L_{iz}^2\omega}\left(\dfrac{1}{L_{iz}} - i(1-a)\beta u_n\right) \\ \dfrac{(1-a)u_n}{L_{iz}} & \dfrac{i(1-a)bu_iu_n}{L_{iz}^2\omega} - i\omega \end{bmatrix} \begin{bmatrix} \tilde{n_n} \\ \tilde{n} \end{bmatrix} = \mathbf{0} \tag{25}$$

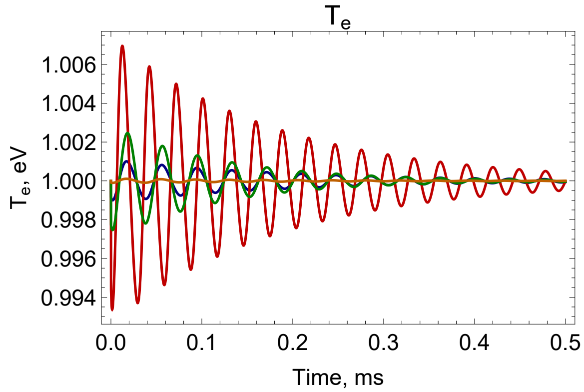

Figure 9. The normalized electron temperature response of the system with Ohm's law included.

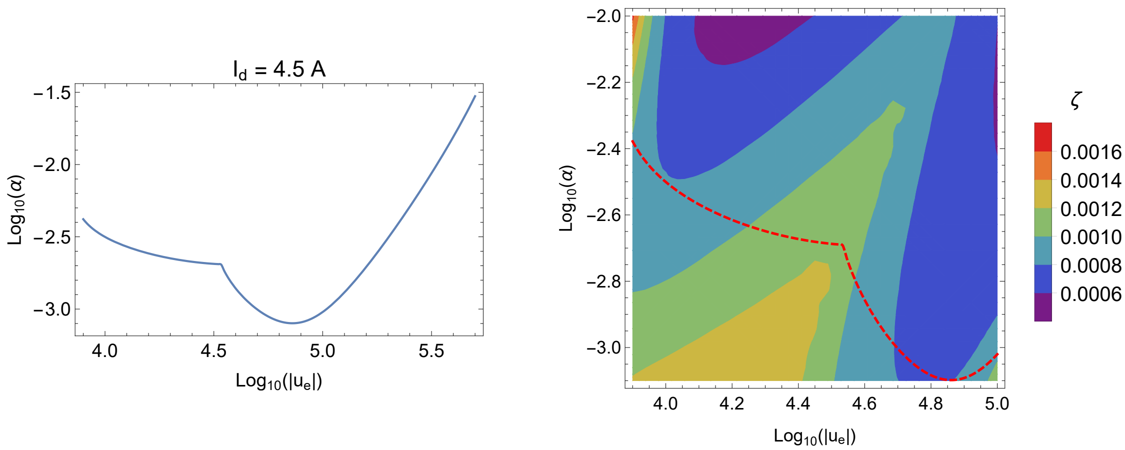

Figure 10. Left: The logarithm of the anomalous collision frequency scaling factor α as a function of the logarithm of u_e in m/s for a nominal discharge current of 4.5 A. Right: The damping ratio of the ion density as a function of the logarithm of u_e in m/s and α, in the vicinity of those values that correspond to the nominal discharge current (red dashed line).

$$i(a-1)bu_iu_n^2 + (a-1)(b-1)L_{iz}u_iu_n\omega + iaL_{iz}^2u_n\omega^2 + L_{iz}^3\omega^3 = 0 \tag{26}$$

For the polynomial $a_0 + a_1s + a_2s^2 + s^3$, the Routh-Hurwitz criteria for stability are $a_0 > 0$, $a_2 > 0$, and $a_1a_2 - a_0 > 0$. For Eq. (26) these criteria become,

$$-\frac{(a-1)bu_iu_n^2}{L_{iz}^3} > 0 \tag{27}$$

$$\frac{au_n}{L_{iz}} > 0 \tag{28}$$

$$\frac{(a-1)u_iu_n^2(a(b-1)-b)}{L_{iz}^3} > 0\ . \tag{29}$$

Given that $\alpha > 1$ and $\beta > 0$, these criteria cannot be satisfied and thus the system is always unstable. However, whether it is purely exponential (such that $\mathrm{Re}(\omega) = 0$) or nonlinearly periodic cannot be determined. However, the simulations of the previous section confirm that the response is periodic for the cases considered.

In order to examine the linear stability numerically, we considered a test case with $u_n \sim 100$ m/s, $u_i \sim 10$ km/s, and $L_{iz} \sim 1$ cm. Fig. 13 shows the growth rate as a function of the logarithm of $a \equiv n_{int}/n_n$ and

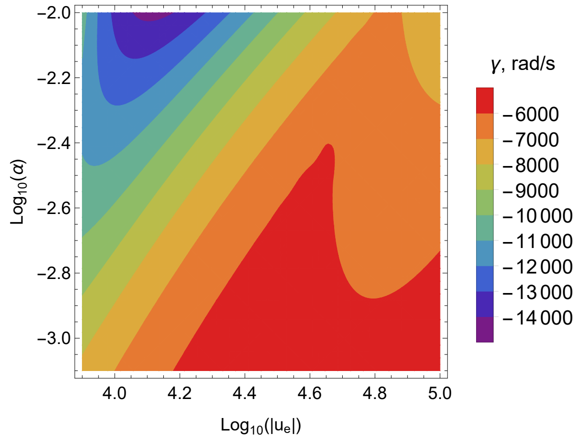

Figure 11. The growth rate of linear perturbations as a function of the logarithm of u_e in m/s and α. Only solutions with a positive real frequency are chosen.

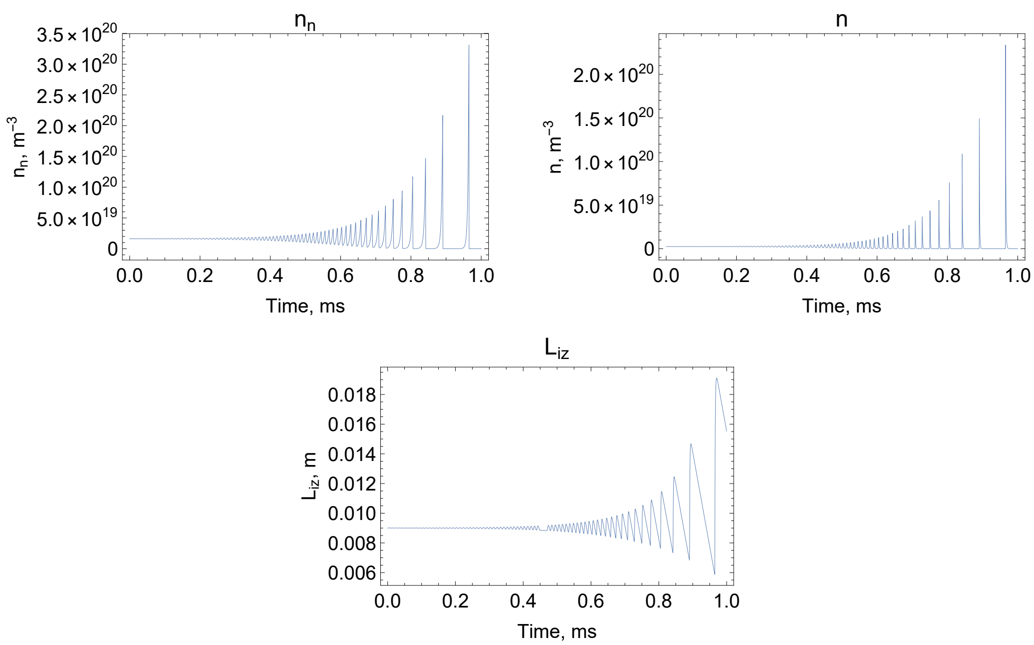

Figure 12. Time response of neutral density, ion density, and ionization length for representative plasma conditions.

$b \equiv \ell/L$ for reasonable ranges of those values: a 10 and b 1, where the latter implies that neutral density drops significantly throughout the entire ionization region. As it shows, the growth rate is everywhere positive. At small b, the growth rate is insensitive to a; at large b, the growth rate is proportional to a. It should be noted that the real frequency for the positive growth region is everywhere zero, indicating the the linear growth is purely exponential and thus any oscillations are a nonlinear effect. Again, the previous numerical simulations confirm this.

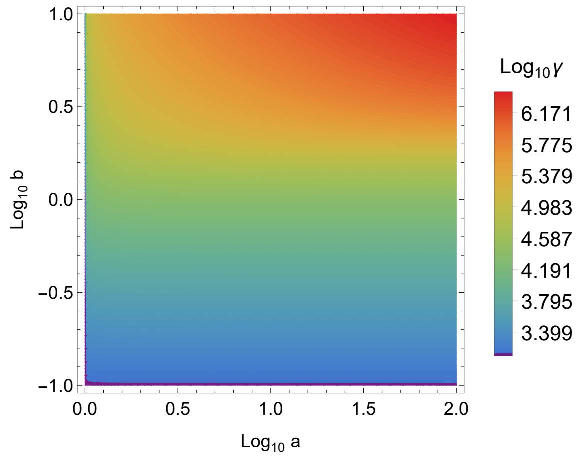

Figure 13. Logarithm of the growth rate in rad/s as a function of the neutral density ratio a and neutral-ionization length ratio b.

V. Discussion

A. Physical Interpretation

It has been shown that the addition of L_{iz} perturbations is sufficient to render the very simple system of Section IV A unstable. It is useful to provide a physical interpretation for this result. To do this, it is important to understand why the continuity equations alone are unconditionally damped. Perhaps the most cogent argument is to note that the time rate of change of n is proportional to that of n_n, and specifically they are 180° out of phase. When the system is perturbed, the system inevitably reaches equilibrium because increases in n (n_n) are immediately met with decreases in n_n (n). Alternatively, L_{iz} perturbations are 90° behind n perturbations. That is, L_{iz} changes to reach equilibrium for the instantaneous n, but by the time L_{iz} has finished deforming, n has changed. This lag, and the attending fact that equilibrium can never be reached, produces growth. The energy source for the instability may be related to the redistribution of energy from the steady, confined ionization region to an unsteady, deforming ionization region.

B. Estimated Growth Rate

An exact form for the real frequency and growth rate of linear perturbation for the model of Section IV E was not derived as part of this work. Without that information, it is difficult to judge whether the nonlinear oscillations observed in Fig. 12 are plausibly breathing mode oscillations. Further, the numerical linear map in Fig. 13 corresponded to roots with zero real frequency, which means the linear analysis can likely not be used to estimate the real frequency because the oscillations are nonlinear in nature. We now prove that the real frequency must always be zero for positive growth of a linear perturbation. If the real part of Eq. (26) is taken given the substitution $\omega = \mathrm{Re}(\omega) + i\gamma$, the following expression results:

$$L_{iz}\mathrm{Re}(\omega)[u_i u_n(a-1)(b-1) + L_{iz}\gamma(2u_n a + 3L_{iz}\gamma)] = 0 \ . \tag{30}$$

Either $L_{iz}\mathrm{Re}(\omega)$ or the term in brackets must equal zero, and assuming that $b \leq 1$ – the neutral density drops entirely within the ionization region – the term in brackets will always be positive. Therefore $\mathrm{Re}(\omega) = 0$ for finite ionization region length.

$$i(a-1)bu_i u_n^2 + (a-1)(b-1)L_{iz}u_i u_n\gamma + iaL_{iz}^2 u_n\gamma^2 + L_{iz}^3\gamma^3 = 0 \tag{31}$$

Assuming positive growth and thus no real frequency, Eq. (26) becomes Eq. (31). Since the second, third, and fourth terms are positive, each of them must be smaller than the first term, which can be used to derive the following relationships:

$$\gamma < \frac{u_n b}{L_{iz}(b-1)} \ , \tag{32}$$

$$\frac{u_i}{u_n} > \frac{ab}{(a-1)(b-1)^2} \approx \frac{b}{(b-1)^2} \gg \frac{b}{b-1} \ . \tag{33}$$

The steady state conditions for the model of Section IV E show that $u_i/u_n = a - 1 \approx a$, and given the condition for the third order term in Eq. (31) to be much smaller than the second order term,

$$a \gg \frac{b}{b-1} \ , \tag{34}$$

we conclude that the third order term may be neglected. What remains can be solved for γ explicitly, where the positive solution is shown as the first expression in Eq. (35). The inequalities previously derived can be applied, yielding the second expression in Eq. (35) as the only definite solution. The term u_i/L_{iz} is more characteristic of the ion transit time instability, which is typically 100 kHz, while the $b - 1/2$ factor reduces the magnitude. It was previously assumed that $b - 1$ is small, which means the growth rate becomes the rightmost expression in Eq. (35). In general, given that it was assumed $\gamma > 0$, a new criterion is presented: $b > 1/2$. The value for $b \equiv \ell/L_{iz}$ is highly dependent on the thruster plasma as a whole, so it is difficult to assess the meaningfulness of this new criterion, or whether it is simply a self-consistent result of the assumption that $b \approx 1$.

$$\gamma = \frac{u_i(a-1)(b-1) \pm \sqrt{u_i(a-1)}\sqrt{u_i(a-1)(b-1)^2 + 4u_n ab}}{2aL_{iz}} \approx \frac{u_i}{L_{iz}}\left(b - \frac{1}{2}\right) \approx \frac{u_i}{2L_{iz}} \tag{35}$$

C. Onset Criteria

Given that the growth rate as estimated in the previous section may be somewhat oversimplified and does not contain a meaningful criterion for the onset of the instability, we must address what this says about the completeness of the model of Section IV E. Although recent analyses[21] of Hall thruster stability delineate "global" oscillations – identified with the breathing mode – and "local" oscillations, it is possible that the linear growth of the breathing mode instability is never completely suppressed but instead changes shape/amplitude due to nonlinear effects or is dominated by other oscillation modes. If this is true, then a criterion that separates positive growth from damping of the breathing mode should not be sought, but instead a scaling law for the growth rate is of interest and should be compared to experimental observations in the range where the breathing mode is dominant. The expression derived in Section V B may constitute such a scaling law, but any experimental validation is reserved for future work.

D. General 0D Limitations

Typical Hall thruster simulation results[22] establish that the plasma varies greatly spatially, indicating that a 0D model is not very useful if it depends on the exact magnitudes of plasma parameters inside the channel, as any average parameters predicted by this model or computed from higher-dimensional models cannot accurately represent the entire channel plasma. For example, the term u_i/L_{iz} often appears in the predator-prey model, and it is assumed that u_i is the beam speed u_{bm}. However, the actual transit time of ions is dictated by the shape of E, which has a strong spatial dependence, and this time will necessarily be less than u_{bm}/L_{iz}. In total, this demonstrates that the choice of plasma parameters for a 0D model is somewhat arbitrary, and thus the results should not strongly depend on the magnitude of these parameters. Previously it was found that many subsets of the governing equations were stable for a wide range of input parameters, and so any instability that they might predict will occur only at very specific magnitudes of the input parameters. As a result, even if some disregarded models predict instability, it may not be a useful result.

VI. Conclusion

In this paper, 0D modeling of the Hall thruster breathing mode was approached numerically and analytically. A temperature-dependent model was first considered, and we found it to be incapable of predicting positive growth. We showed that the electron energy equation was largely decoupled from the rest of the system in the current 0D formulation, which is unconditionally stable according to a Routh-Hurwitz stability analysis. Adding Ohm's law to the model did not improve this coupling and rendered the system dependent on u_e and I_d or α, but it was still found unconditionally stable for the specific cases examined. Finally, we returned to the traditional predator-prey model except ionization length was assigned a perturbed form by considering the motion of the upstream edge of the ionization region. The resulting model is less complicated than the temperature-dependent model and amenable to Routh-Hurwitz analysis, which shows it to be unconditionally unstable. Numerical simulations support this conclusion, and the derivation of an approximate growth rate was explored.

Acknowledgments

This work is partly supported by NASA Space Technology Research Fellowship grant NNX14AL65H. E. Dale would like to thank Dr. Yiangos Mikellides for the opportunity to work with him on modeling the breathing mode and the fruitful discussions that followed.

References

[1] Hara, K., Sekerak, M. J., Boyd, I. D., and Gallimore, A. D., "Perturbation analysis of ionization oscillations in Hall effect thrusters," *Physics of Plasmas (1994-present)*, Vol. 21, No. 12, Dec. 2014.

[2] Oh, D. Y., Snyder, J. S., Goebel, D. M., Hofer, R. R., and Randolph, T. M., "Solar Electric Propulsion for Discovery-Class Missions," *Journal of Spacecraft and Rockets*, Vol. 51, No. 6, 2014, pp. 1822–1835.

[3] Diamant, K., Spektor, R., Beiting, E., Young, J., and Curtiss, T., "The Effects of Background Pressure on Hall Thruster Operation," *48th AIAA/ASME/SAE/ASEE Joint Propulsion Conference & Exhibit*, American Institute of Aeronautics and Astronautics, Atlanta, GA, July 2012.

[4] Frieman, J. D., Walker, J. A., Walker, M. L. R., Khayms, V., and King, D. Q., "Electrical Facility Effects on Hall Thruster Cathode Coupling: Performance and Plume Properties," *Journal of Propulsion and Power*, Vol. 32, No. 1, 2016, pp. 251–264.

[5] Adam, J. C., Hron, A., and Laval, G., "Study of stationary plasma thrusters using two-dimensional fully kinetic simulations," *Physics of Plasmas*, Vol. 11, No. 1, Dec. 2003, pp. 295–305.

[6] Koo, J. W. and Boyd, I. D., "Modeling of anomalous electron mobility in Hall thrusters," *Physics of Plasmas*, Vol. 13, No. 3, March 2006, pp. 033501.

[7] Fife, J., Martinez-Sanchez, M., and Szabo, J., "A numerical study of low-frequency discharge oscillations in Hall thrusters," *33rd AIAA/ASME/SAE/ASEE Joint Propulsion Conference and Exhibit*, American Institute of Aeronautics and Astronautics, July 1997.

[8] Boeuf, J. P. and Garrigues, L., "Low frequency oscillations in a stationary plasma thruster," *Journal of Applied Physics*, Vol. 84, No. 7, Oct. 1998, pp. 3541–3554.

[9] Bareilles, J., Hagelaar, G. J. M., Garrigues, L., Boniface, C., Boeuf, J. P., and Gascon, N., "Critical assessment of a two-dimensional hybrid Hall thruster model: Comparisons with experiments," *Physics of Plasmas*, Vol. 11, No. 6, May 2004, pp. 3035–3046.

[10] Barral, S. and Peradzyski, Z., "Ionization oscillations in Hall accelerators," *Physics of Plasmas (1994-present)*, Vol. 17, No. 1, Jan. 2010.

[11] Coche, P. and Garrigues, L., "A two-dimensional (azimuthal-axial) particle-in-cell model of a Hall thruster," *Physics of Plasmas*, Vol. 21, No. 2, Feb. 2014.

[12] Hara, K., *Development of Grid-Based Direct Kinetic Method and Hybrid Kinetic-Continuum Modeling of Hall Thruster Discharge Plasmas.*, Ph.D. thesis, University of Michigan, 2015.

[13] Choueiri, E. Y., "Plasma oscillations in Hall thrusters," *Physics of Plasmas (1994-present)*, Vol. 8, No. 4, April 2001, pp. 1411–1426.

[14] Sekerak, M. J., Longmier, B., Gallimore, A., Huang, W., Kamhawi, H., Hofer, R. R., Jorns, B., and Polk, J. E., "Mode Transitions in Magnetically Shielded Hall Effect Thrusters," *50th AIAA/ASME/SAE/ASEE Joint Propulsion Conference*, American Institute of Aeronautics and Astronautics, Cleveland, OH, July 2014.

[15] McDonald, M. S. and Gallimore, A. D., "Comparison of breathing and spoke mode strength in the H6 Hall thruster using high speed imaging," *33rd International Electric Propulsion Conference*, Washington DC, USA, Oct. 2013.

[16] MacDonald-Tenenbaum, N., Young, C. V., Fabris, A. L., Nakles, M., Hargus Jr, W., and Cappelli, M. A., "Time-Synchronized Continuous Wave Laser Induced Fluorescence Velocity Measurements of a 600 Watt Hall Thruster," *34th International Electric Propulsion Conference*, Air Force Research Lab Edwards AFB Aerospace Systems Directorate, Kobe, Japan, July 2015.

[17] Barral, S. and Ahedo, E., "On the Origin of Low Frequency Oscillations in Hall Thrusters," *AIP Conference Proceedings*, Vol. 993, AIP Publishing, March 2008, pp. 439–442.

[18] Barral, S. and Ahedo, E., "Low-frequency model of breathing oscillations in Hall discharges," *Physical Review E*, Vol. 79, No. 4, April 2009.

[19] Hurwitz, A., "On the conditions under which an equation has only roots with negative real parts," *Selected papers on mathematical trends in control theory*, Vol. 65, 1964, pp. 273–284.

[20] Garner, C., Brophy, J., Polk, J., and Pless, L., "Cyclic endurance test of a SPT-100 stationary plasma thruster," *30th Joint Propulsion Conference and Exhibit*, American Institute of Aeronautics and Astronautics, 1994, DOI: 10.2514/6.1994-2856.

[21] Sekerak, M. J., Gallimore, A. D., Brown, D. L., Hofer, R. R., and Polk, J. E., "Mode Transitions in Hall-Effect Thrusters Induced by Variable Magnetic Field Strength," *Journal of Propulsion and Power*, Vol. 32, No. 4, 2016, pp. 903–917.

[22] Parra, F. I., Ahedo, E., Fife, J. M., and Martnez-Snchez, M., "A two-dimensional hybrid model of the Hall thruster discharge," *Journal of Applied Physics*, Vol. 100, No. 2, July 2006, pp. 023304.